Earth Planet. Sci. Lett. 668 (2025) 119543

Contents lists available at ScienceDirect

Earth and Planetary Science Letters

journal homepage: www.elsevier.com/locate/epsl

An abrupt change in source materials for Chinese loess deposits at the Pliocene-Pleistocene boundary: Insights from K isotopes and modeling

Jun Mu [a,c], Jiawei Da [b,d], Hu Yang [e], Junfeng Ji [b], Lianwen Liu [b], Weiqiang Li [a,c,*]

[a] State Key Laboratory of Critical Earth Material Cycling and Mineral Deposits, School of Earth Sciences and Engineering, Nanjing University, Nanjing 210023, China
[b] Ministry of Education Key Laboratory of Surficial Geochemistry, School of Earth Sciences and Engineering, Nanjing University, Nanjing 210023, China
[c] Frontiers Science Center for Critical Earth Material Cycling, Nanjing University, Nanjing 210023, China
[d] Department of Earth and Planetary Sciences, The University of Texas at Austin, Austin, TX 78712, USA
[e] Southern Marine Science and Engineering Guangdong Laboratory, Zhuhai, China

ARTICLE INFO

Edited by: Dr Y Asmerom

Keywords:
Potassium isotopes
Eolian deposits
Chinese Loess Plateau
East Asian atmospheric circulation
Quaternary cooling
Earth system modeling

ABSTRACT

The eolian deposits on the Chinese Loess Plateau (CLP) are key archives of late Cenozoic climate changes and atmospheric circulation, However, the long-standing controversy about the stability of dust sources over the last ~ 6 Myr limits our understanding of the genesis of the CLP and its paleoenvironment implications. Here we report that an abrupt decrease in K isotope compositions ($\delta^{41}K$) of the CLP eolian deposits occurred at ~2.58 Ma, with loess/paleosol displaying $\delta^{41}K$ values (-0.41 ‰ to -0.63 ‰) lower than the bulk-silicate-earth-like Red Clay values (-0.35 ‰ to -0.45 ‰). Furthermore, The $\delta^{41}K$ values of eolian deposits are negatively correlated with the Na_2O/K_2O and Na_2O/Al_2O_3 ratios, with negligible influence from different grain size fraction. These observations indicate that the $\delta^{41}K$ values are not controlled by post-depositional weathering at the CLP, but rather by an increased export of weathered detritus or recycled sediments from the Northeastern Tibetan Plateau, as revealed by K isotope surveys of potential source materials and Earth system model simulations. Our results further suggest that the intensified global cooling during the Quaternary promoted greater sediments erosion and altered the dynamics of the westerlies and the Siberian High, with important implications for understanding the paleoenvironment changes and reconstruction of the East Asian atmospheric circulation across the Pliocene-Pleistocene boundary.

1. Introduction

The Chinese Loess Plateau (CLP) in northern China hosts the most extensive and complete eolian deposits in the world. These eolian deposits, with thicknesses of ~150 to ~300 m, provide a unique record of East Asian atmospheric circulation and paleoclimate during the late Cenozoic. The wind-blown deposits bear dust-source information, and changes in the source materials could disturb the proxy-based (e.g., magnetic susceptibility, grain size, geochemical proxies) paleoclimate reconstructions (Chen and Li, 2011). Elucidating the sources of the eolian deposits not only has implications for paleo-environmental reconstructions but also enhances our understanding of the atmospheric circulation pattern over inland Asia that eventually gave rise to the CLP.

The eolian deposits of CLP can be broadly separated into the lower Red Clay Formation (~8 to 2.58 Ma) and the upper loess-paleosol sequence (~ 2.58 to 0 Ma). A number of studies have focused on the provenance of Quaternary loess-paleosol sequence (Bird et al., 2020; Licht et al., 2016; Nie et al., 2015; Stevens et al., 2013; Xiao et al., 2012; Zhang et al., 2016; Zhou et al., 2022), which suggested a dominant source from the Northeastern Tibetan Plateau (NTP) with contribution from central Asian orogenic belt. However, the temporal changes in the source materials of the CLP remain a contentious issue. Sr--Nd--Pb isotopic data of the Jingchuan section indicate a dramatic source change over the last ~2.58 Myr (Sun, 2005; Sun and Zhu, 2010). By contrast, Sr-Nd isotope analyses from the Lingtai section implied a constant source over the last ~7 Myr (Bird et al., 2020; Wang et al., 2007). Although the Hf isotope data indicated an unchanged source at certain stages, such as 2.5 Ma, 1.2 Ma and last (inter)glacial period in the Lingtai section, a prominent decrease in Hf isotope values were observed between 0–1.2 Ma (Bird et al., 2020; Chauvel et al., 2014). Moreover, oxygen isotope analyses of quartz in the Lingtai section revealed significant dust composition changes and unstable dust sources at 2.6 Ma

* Corresponding author.
E-mail address: liweiqiang@nju.edu.cn (W. Li).

https://doi.org/10.1016/j.epsl.2025.119543
Received 11 February 2025; Received in revised form 22 May 2025; Accepted 10 July 2025
Available online 18 July 2025

and 1.2 Ma, respectively (Yan et al., 2017). To date, a comprehensive investigation into the provenance evolution of eolian deposits and corresponding source materials throughout the Plio-Pleistocene on the CLP are scarce and remain essential.

The discrepancy among provenance studies of the CLP based on traditional tracers could be due to bias introduced by transport sorting effect. For instance, $^{87/86}$Sr ratios are susceptible to weathering and sorting effects (Rao et al., 2006), and Hf isotope would be largely affected by zircons due to high chemical affinity between Zr and Hf. For provenance studies involving zircon U-Pb age spectra, a source bias may be introduced into the high-density coarse zircon grains (> 25 μm) as a result of dust sorting and recycling (Zhang et al., 2022), and a similar issue can occur within other heavy minerals. Here, we aim to complement traditional methods by employing potassium (K) isotopes, a novel geochemical tool, to provide a new perspective in tracing source materials for the CLP, thereby enhancing our understanding of the genesis of the CLP and East Asia atmospheric circulation changes over the last ~6 Myr.

Potassium is the eighth most abundant element in the Earth's crust and is enriched in silicates that dominate the CLP deposits. Notably, due to the negligible K content in carbonates, the K isotope values of sediments are immune to the presence of carbonate (Fig. S1; text S1), a common issue for other geochemical proxies on the CLP (e.g., ^{87}Sr/^{86}Sr, δ^{26}Mg). The significant K isotopic fractionation in surface environments (e.g., Huang et al., 2020; Mu et al., 2024; Teng et al., 2020) and the general K isotopic homogeneity in igneous rocks (Hu et al., 2021) should provide new insights into the formation of the CLP and paleoenvironment changes from the eolian dust record.

In this study, we performed the first systematic investigation of the K isotope composition (δ^{41}K) in samples from two classic loess-Red Clay sequences (Lingtai and Lantian sections) on the CLP, as well as the CLP's potential source materials across the regions of northern and northwestern China. These data are compiled and compared in a context of Earth system model simulation results for the regions, which suggests that an increased contribution of weathered materials to the CLP occurred ~2.58 Ma due to global cooling. The new constraints on the source of the CLP have important implications for understanding the land-atmosphere interaction and the Asian atmospheric circulation in the late Cenozoic.

2. Materials and methods

2.1. Samples collection and grain size separation

Bulk samples from the upper loess-paleosol sequence and lower Red Clay were sequentially collected from the CLP (Fig. 1). Forty-two and thirty-three eolian dust samples were obtained from the Lantian section (134.15°E, 34.15°N) and the Lingtai section (107.62°E, 35.07°N), respectively. The Lantian and Lingtai sections, located in Shaanxi and Gansu Provinces respectively, represent two critical terrestrial archives of East Asian paleoclimate and tectonic evolution. The Lantian profile, situated on the northern terrace of the Bahe River near the Qinling Mountains, preserves approximately 60 m of Red Clay and ~120 m of Quaternary loess with well-developed paleosol layers (e.g., S5) that record paleo-environmental changes (Zheng et al., 1992). Similarly, the Lingtai section, located at the south-central CLP, is characterized by the thickest and continuous eolian deposits (~300 m), comprising 170 m of Quaternary loess-paleosol and 126 m of Pliocene Red Clay (Ding et al., 1999). These two sections have been extensively studied to reconstruct the history of global cooling, East Asian monsoon dynamics, and Tibetan plateau uplift since ~7 Ma.

The geochronology of the loess-paleosol and Red Clay sequences for both sections was well established by magnetic reversal stratigraphy (Da et al., 2023; Sun et al., 2010). In addition, seventy-four surficial desert samples and riverine sediments were collected from the Mongolian Gobi, Tarim Basin, Junggar Basin, Qaidam Basin, Tengger Desert, Ordos Desert, the upper reaches of the Yellow River, and rivers draining the Qilian Mountains (i.e., the Ruoshui River and Shiyang River). To evaluate the particle-size effect on K isotopes, twelve loess and paleosol samples (six each) were separated into different grain-size fractions (i.e., < 2 μm, 2–25 μm, 25–43 μm, > 43 μm) by wet sieving, and the < 2 μm fraction of the four Red Clay samples were also measured. The bulk samples used to test grain size effect were collected from different sections across the CLP, namely Huanxian section, Fuxian section, Jingchuan section, Xifeng section, Lingtai section, and Lantian section (Fig. S2).

For those samples requiring grain size separation, approximately 2–3 g of loess and paleosol were soaked in Milli-Q water for 12 h with ultrasonic treatment to disaggregate fine particles. The size fractions of > 43 μm, 25–43 μm were separated by wet sieving. The remaining < 25 μm

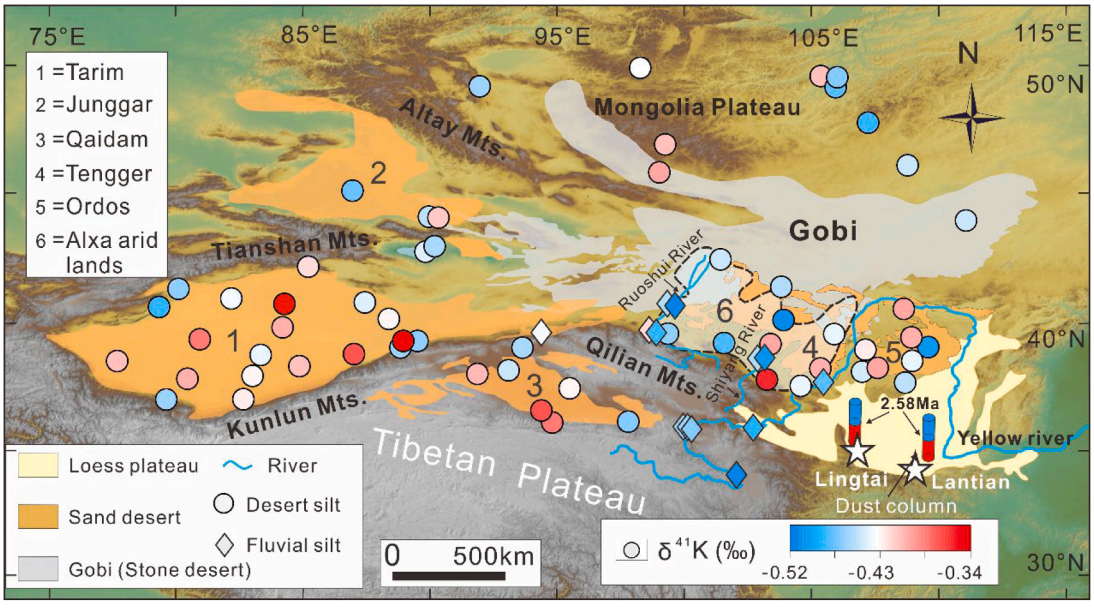

Fig. 1. Map showing the extent of the CLP and the potential dust-emitting source regions. The stars mark the sampling locations of the Red Clay and loess-paleosol sequence on the CLP.

fractions were decanted into the SHMP (sodium hexametaphosphate (dispersant) + Milli-Q water mixture) solution, well mixed and standing for 16 h in a 1 L beaker. Clay fraction (< 2 μm) and 2–25 μm fraction were recovered by sampling top 3 cm solutions and settled particles, respectively (Guinoiseau et al., 2016). Additionally, considering the dust transport capacity of wind, desert silts and riverine silts fractions (< 63 μm) were recovered by wet sieving as it takes up > 80 % of the loess particles (Ding et al., 1999). Each fraction was dried at 50–60°C followed by washing and centrifugation several times using Milli-Q water until no detectable K in the supernatants. After that, the solid samples were transferred into beakers and dissolved with double-distilled concentrated HF + HNO_3 and aqua regia (3 mL HCl + 1 mL HNO_3) prior to chemical purification by two-stage column chromatography (An et al., 2022).

2.2. Analytic methods

2.2.1. Potassium isotope analysis

The bulk samples and different size fractions were placed in screw-top Teflon beakers and sequentially dissolved with double-distilled 3 mL concentrated HF + HNO_3 and aqua regia (3 mL HCl + 1 mL HNO_3) on a hotplate at 130°C for 48 h. After that, all the dissolved samples were dried and re-dissolved in 2 mL 2 % HNO_3 (v/v). A 0.2 mL aliquot of the solution was taken and diluted into 3 mL 2 % HNO_3 (v/v) for elemental analysis by flame photometer. Based on the element concentrations, one aliquot of the sample solution containing ~20 μg of K was transferred into new beakers that dried at 95°C, and re-dissolved three times in 0.1 mL concentrated HNO_3 to transform cations to nitrate form. Lastly, the sample was heated to dryness and dissolved in 100 μL of 1.0 mol/L HNO_3 solution prior to chemical purification using the two-stage column protocol.

Potassium isotope analysis was performed on a Nu 1700 Sapphire High-Resolution Multi-Collector Inductively Coupled Plasma Mass Spectrometer (HR-MC-ICP-MS) at the State Key Laboratory for Mineral Deposits Research, Nanjing University, China, following the method described in detail by An et al. (2022). The instrument was running at a dry and hot plasma conditions, with a standard 1300 W forward RF power. An Aridus III desolvating system was used for sample introduction. Standard–sample bracketing (SSB) method was used to correct mass bias and instrumental drift, with each K sample bracketed by a 200 ppb in-house K isotope standard (A-K). The $\delta^{41}K$ value of the in-house standard (A-K) relative to NIST 3141a is −0.05 ± 0.07 ‰ (2SD, n = 120) (An et al., 2023). The long-term external reproducibility of the K isotope analyses in our lab is better than 0.06 ‰ (2SD). The K isotopic ratios ($^{41}K/^{39}K$) were expressed as a delta notation relative to international K isotope standard solution NIST 3141a:

$$\delta^{41}K_{NIST\ 3141a}\ (‰) = [(^{41}K/^{39}K)_{sample} / (^{41}K/^{39}K)_{NIST\ 3141a} - 1] \times 1000$$

The Atlantic seawater and the USGS rock standard GSP-2 were regarded as unknown samples for validating the accuracy of the total chemical and mass spectrometry procedures. The K isotope compositions of measured natural standards ($\delta^{41}K_{seawater}$ =0.11± 0.04 ‰ and $\delta^{41}K_{GSP\text{-}2}$ =−0.42± 0.06 ‰) are consistent with the literature results within uncertainty (Hu et al., 2018; Morgan et al., 2018).

2.2.2. Major elements analysis

The major-element compositions of the Red Clay, loess, and paleosol were determined using a Thermo Scientific ARL 9900 X-ray fluorescence spectrometer at the State Key Laboratory for Mineral Deposits Research, Nanjing University. The instrument was operated at an accelerating voltage of 40 kV, with a 70 mA focusing beam and the peak counting times of 20 s. Natural standard materials BHVO-2 and BCR-2 were used for instrument monitoring and calibration. The long-term external uncertainty of major element analyses was better than ±3 % (2RSD) for major oxides (SiO_2, Al_2O_3, Fe_2O_3, MgO, CaO, K_2O, Na_2O) and ±10 % (2RSD) for trace oxides (e.g., P_2O_5).

2.3. Climate model simulations

The onset of the Quaternary period was characterized by a notable decline in atmospheric CO_2 pressure (Fig. 2a), increase in benthic oxygen isotope values (Fig. 2b), and the major intensification of Northern Hemisphere glaciation (iNHG) (Rae et al., 2021). To explore the cooling effects on environmental factors (e.g., land surface humidity, atmospheric dynamics) influencing dust production and transport, we performed two simulations using Alfred Wegener Institute-Earth System Model (AWI-ESM) to reconstruct the impact of global cooling on the regional climate (Sidorenko et al., 2019). The first experiment applied a relatively high greenhouse gas forcing (pCO_2=568 ppmv) to simulate a warmer climate. The second experiment operates with CO_2 forcing at pre-industrial level (284 ppmv). The other boundary conditions, such as land-sea distribution and ice sheet configuration, are kept the same as present-day (see details in Text S2). Comparison between these two experiments illustrates the climate changes under global cooling.

3. Results

3.1. K isotope compositions of eolian deposits and source materials

The $\delta^{41}K$ values of eolian deposits vary from −0.35 ‰ to −0.63 ‰ in the two classic sections (Fig. 2 and Table S1). Notably, the measured $\delta^{41}K$ values for samples from the Lantian (−0.38 ‰ to −0.62 ‰) and Lingtai sections (−0.35 ‰ to −0.63 ‰) show similar range, variability, and trend (Fig. 2). The Red Clay samples exhibit homogeneous $\delta^{41}K$ values in both the Lantian section (−0.41 ± 0.03 ‰, 2SD, n = 14) and Lingtai section (−0.42 ± 0.06 ‰, 2SD, n = 7), which are overall ~0.2 ‰ higher than those of the overlying Quaternary loess-paleosol sequences in both sections. Four grain size fractions (i.e., < 2 μm, 2–25 μm, 25–43 μm, > 43 μm) of each sample show consistent $\delta^{41}K$ values considering the analytical errors (Fig. 3 and Table S2). Major element concentrations of loess-Red Clay samples are within the range of previous studies . The ratios of Na_2O/K_2O and Na_2O/Al_2O_3 display a positive trend since the last ~ 6 Ma (Fig. S3 and Table S3), and the K isotope values of eolian deposits show negative correlations with both Na_2O/K_2O and Na_2O/Al_2O_3 (Fig. 3). Moreover, the $\delta^{41}K$ values of Quaternary loess-paleosol sequence fall within the range of those from upper continental crust materials (e.g., soil, weathered silicates) (Fig. 4).

The $\delta^{41}K$ values of deserts samples vary from −0.36 ‰ to −0.51 ‰, and the Red Clay-like, high $\delta^{41}K$ (−0.36 ‰ to −0.42 ‰) are observed surrounding the NTP area, namely Tarim Basin, Qaidam desert and Tengger desert. Additionally, the fluvial sediments from the upper reaches of Yellow River, Ruoshui River and Shiyang River exhibit the loess-like low $\delta^{41}K$ values (−0.42 ‰ to −0.51 ‰) (Fig. 5 and Table S4).

3.2. Modelling results

Simulation results show that under cooling conditions, previously arid regions experience an increase in net humidity, as the reduction in evaporation exceeds that of precipitation (Fig. 6a). This creates favorable conditions for the production of fine-grained weathering particles (Zhang et al., 2019; Zhong et al., 2022). On the other hand, climate simulations indicate that the westerly winds experienced a significant southward shift at the low-CO_2 condition, accompanied by a strengthened Siberian High. This change leads to a weakening of westerly winds over the Tarim Basin, while over the east of NTP region, the westerlies intensified. The reinforcement of the northeast winds, driven by the strengthened northern Siberian High and westerlies (Fig. 6b), likely facilitated the transport of dust from desert regions surrounding the CLP.

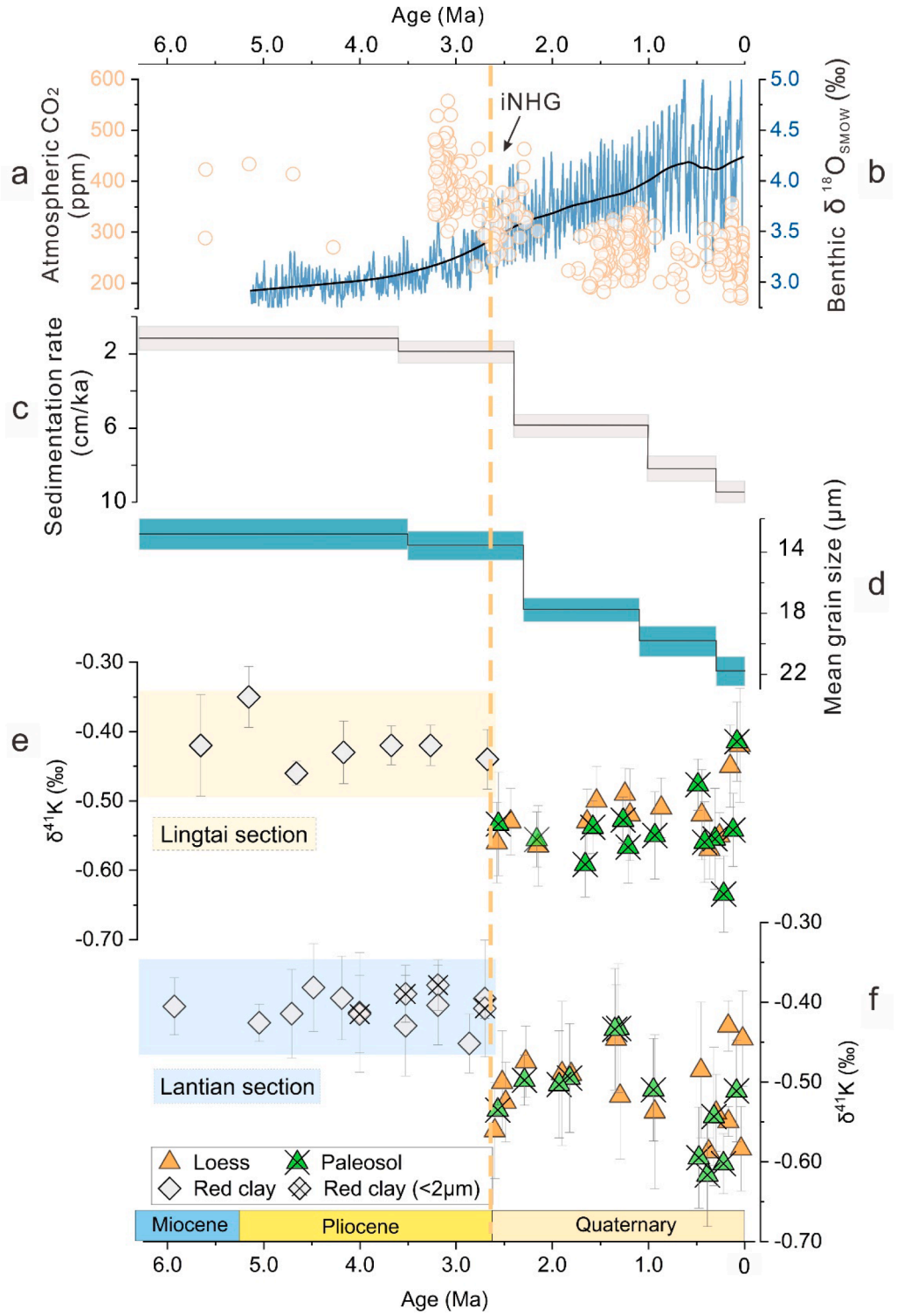

Fig. 2. Temporal evolution of K isotope values compared with other geological records. (**a**). Atmospheric CO_2 record (Rae et al., 2021). (**b**). LR04 benthic oxygen isotope record (Lisiecki and Raymo, 2005). (**c, d**). Increasing in dust sedimentation rate and mean grain size of the eolian deposits (Lu et al., 2010). (**e, f**). K isotope compositions of loess-Red Clay sequences in Lingtai section and Lantian section, respectively. The error bar refers to two standard deviations.

4. Discussion

4.1. Provenance control on K isotopic variation of eolian deposits

Approximately 0.2 ‰ difference in $\delta^{41}K$ between Red Clay and loess-paleosol deposits is significantly greater than the external reproducibility of K isotope analysis (± 0.06 ‰) (An et al., 2022), and the difference between the two groups of samples (i.e., the Red Clay before 2.58 Ma and the loess-paleosol in recent 2.58 Ma) is not only visually evident in Fig. 2, but also statistically significant as shown by two-tailed student's *t*-test (P-value << 0.001 at 95 % confidence level).

The decrease in $\delta^{41}K$ of the loess-paleosol sequence cannot be caused by post-depositional weathering of isotopically homogeneous eolian deposits. The chemical alteration occurring after dust accumulation

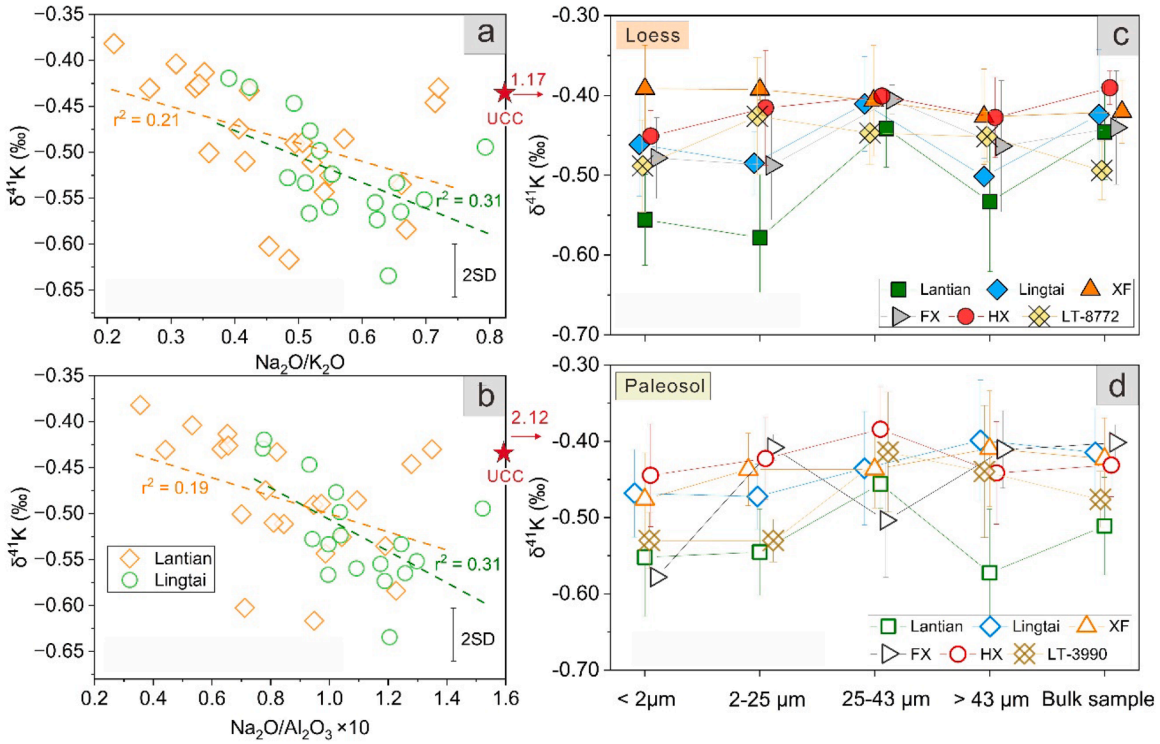

Fig. 3. Plots of K isotope variation versus the chemical weathering indices Na_2O/K_2O (a), Na_2O/Al_2O_3 (b), and different grain-size fractions. (**c**). The $\delta^{41}K$ values of the loess samples L1 across the CLP and the L15 (1.25 Ma) sample LT-8772 from Lingtai section. (**d**). The $\delta^{41}K$ values of the paleosol samples S1 across the CLP and the S5 (0.49 Ma) sample LT-3990 from Lingtai section. 2SD: Two Standard Deviation. UCC: Upper Continental Crust.

generally involves: (1) weathering of primary minerals (e.g., leaching); and 2) enhanced pedogenesis under warmer/wetter interglacial climates that transforms loess into paleosol. It has been documented that gradual weakening in chemical weathering intensity occurred since the Late Miocene, as evidenced by the increase of dust mean grain size (Lu et al., 2010), element ratios (e.g. Na_2O/K_2O, Na_2O/Al_2O_3), and drop in chemical index of alteration values (Xiong et al., 2010; Yang et al., 2021). During silicate weathering, the weathered residues tend to have lower $\delta^{41}K$ values due to preferential retention of ^{39}K in secondary minerals (Chen et al., 2020; Teng et al., 2020). Besides, Na_2O/K_2O and Na_2O/Al_2O_3 ratios of eolian deposits can serve as weathering intensity proxies because of the more readily degradation of plagioclase than K-feldspar in dust deposits (Chen et al., 2001). Hence, the greater the degree of chemical weathering, the lower the Na_2O/K_2O and Na_2O/Al_2O_3 ratios, and the more negative the $\delta^{41}K$ values. However, the $\delta^{41}K$ values of eolian dust are reversely correlated with the Na_2O/K_2O and Na_2O/Al_2O_3 ratios (Fig. 3a, b; and Table S2), contradicting the trend of K isotope variability in weathered residues (Mu et al., 2024; Teng et al., 2020). In addition, within the loess-paleosol sequence, the paleosol units show nearly identical $\delta^{41}K$ values to that of coeval loess units (Fig. 2), with $\Delta^{41}K_{paleosol\text{-}loess}$ ($\delta^{41}K_{paleosol}$-$\delta^{41}K_{loess}$) mostly within ±0.05 ‰ (Fig. S4). These collectively suggest that the post-depositional weathering has had a negligible impact on the decline in $\delta^{41}K$ values observed in the eolian deposits.

Another line of evidence of non-post-depositional weathering control comes from the grain size-related $\delta^{41}K$ results. Chemical weathering leads to higher content of clays in residues that are characterized by lower $\delta^{41}K$ values (Teng et al., 2020). If the observed low $\delta^{41}K$ values in loess and paleosol result from the post-depositional weathering, the clay-rich fine-sized fraction of these samples would be more enriched in light K isotopes. However, the $\delta^{41}K$ values of the bulk loess-paleosol samples are barely distinguishable from those of the different size fractions (i.e., < 2 μm, 2–25 μm, 25–43 μm, > 43 μm), and each size fraction displays almost no difference in $\delta^{41}K$ values considering analytical errors (Fig. 3c and d), despite a few samples that show slightly lower $\delta^{41}K$ values in the clay-size fraction (< 2 μm). This may be due to the neoformation of clay minerals during pedogenesis (Text S3, Fig. S4, S5). Overall, the negligible effect of grain size on $\delta^{41}K$ values rules out the post-depositional weathering control on the $\delta^{41}K$ values of loess and Red Clay.

Changes in $\delta^{41}K$ values of the eolian deposits across the Pliocene-Pleistocene boundary are broadly synchronous with increases in both dust accumulation rates and mean grain size (Fig. 2c, and d), accompanying changes in mineral assemblages of eolian dust as a result of source materials change (Gyllesjö and Arnold, 2006; Yan et al., 2017). Specifically, previous study has documented systematic differences in the abundance of major K-bearing minerals (i.e., plagioclase, orthoclase, mica) between the Red Clay and loess-paleosol sequence at the Lingtai section (He et al., 2017; Fig. S6). The Red Clay contains lower proportions of plagioclase (12–14 %) and mica (1–4 %) compared to the overlying loess–paleosol deposits, which are enriched in these phases (plagioclase: 13–17 %; mica: 4–8 %). Moreover, the orthoclase contents remain roughly comparable or show a decrease from the Red Clay to the loess–paleosol sequence, and a pronounced reduction in the clay-sized fraction (<2 μm) is observed in the loess/paleosol deposits (Gyllesjö and Arnold, 2006). Beyond the mineralogical difference, the similarity in $\delta^{41}K$ values between the Quaternary L1-S1 units and Red Clay (Fig. 2e and f), alongside similar patterns identified in Nd-Hf isotopes (Bird et al., 2020; Chen and Li, 2013) and rare earth elements studies (Ding et al., 2001), further supports a provenance control on the K isotope values. Collectively, these observations suggest that changes in dust source materials, rather than post-depositional chemical weathering or grain size sorting effects, exert a first-order control on the $\delta^{41}K$ values of eolian deposits over the past ~ 6 Myr.

The provenance control on $\delta^{41}K$ values of eolian deposits also provide explanation for the observed negative trend between $\delta^{41}K$ values and Na_2O/K_2O and Na_2O/Al_2O_3 ratios. Previous studies have also documented that the Na_2O/Al_2O_3 ratios of dust are size-dependent (Ding

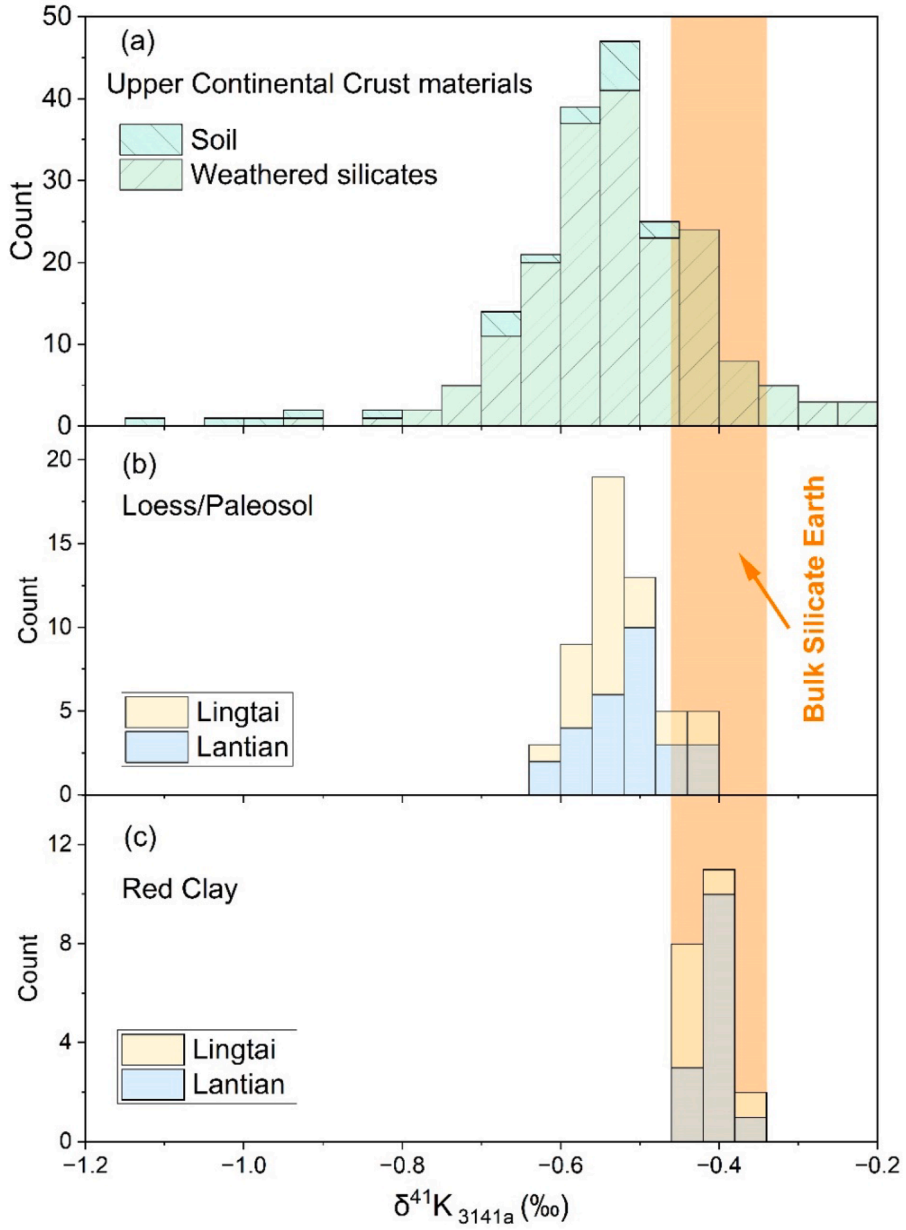

Fig. 4. Comparison of $\delta^{41}K$ signatures among (a) upper continental crust materials, (b) Quaternary loess/paleosol, and (c) Red Clay. The upper continental crust materials include sedimentary rocks (Morgan et al., 2018; Li et al., 2019; Huang et al., 2020), soil (Li et al., 2021; Li et al., 2022), river sediments (Li et al., 2019a; Li et al., 2022), residues of weathering profiles (Chen et al., 2020; Teng et al., 2020) and terrestrial shallow-sea shelf sediments (Mu et al., 2024). The $\delta^{41}K$ value of the bulk silicate earth (BSE) is from Hu et al. (2021).

et al., 2001; Li et al., 2025; Xiong et al., 2010), with finer-grained fractions exhibiting much lower Na_2O/Al_2O_3 ratios (Yang et al., 2006). This observation aligns with well-established textural differences between the deposits. Red Clay units display characteristically finer grain sizes (median: <10 μm) with a higher proportion of clay-sized particles (20–30 % of <2 μm fraction), while loess-paleosol sequence is consistently coarser (median: 10–25 μm) and contain reduced clay-sized fractions (~10 %) (Gylesjö and Arnold, 2006; Xiong et al., 2010). Thus, the negative trend between $\delta^{41}K$ values and Na_2O/K_2O and Na_2O/Al_2O_3 ratios can be best interpreted as the result of binary mixing between two endmembers: (i) a clay fraction-rich component with bulk silicate Earth-like $\delta^{41}K$ values and low Na_2O/Al_2O_3 ratios and (ii) a silt-dominated component characterized by lower $\delta^{41}K$ values and relatively higher Na_2O/Al_2O_3 ratios. It should be noted that the Na_2O/K_2O ratio acts as a proxy analogous to Na_2O/Al_2O_3 ratio herein, given that the K_2O/Al_2O_3 ratio is largely insensitive to grain-size variations (Li et al., 2025).

4.2. *Tracing dust source for the CLP eolian deposits*

Deserts located in the distal inland basins (e.g., the Tarim basin and Qaidam basin) and proximal deserts (e.g., the Tengger Desert, the Ordos Desert) have been argued as major dust source regions of the CLP (Chen and Li, 2011). Modern desert silts have been broadly utilized for identifying source regions, as their chemical signatures are not readily altered (e.g., Chen and Li, 2011; Li et al., 2018). Additionally, deserts in Ansian interior are continuously rejuvenated by accommodating erosional products from adjacent mountains (Lu et al., 2019), thereby maintaining representative regional geochemical signatures. Consequently, K isotope compositions preserved in desert silts may offer valuable additional constraints on the identification of dust-emitting source regions.

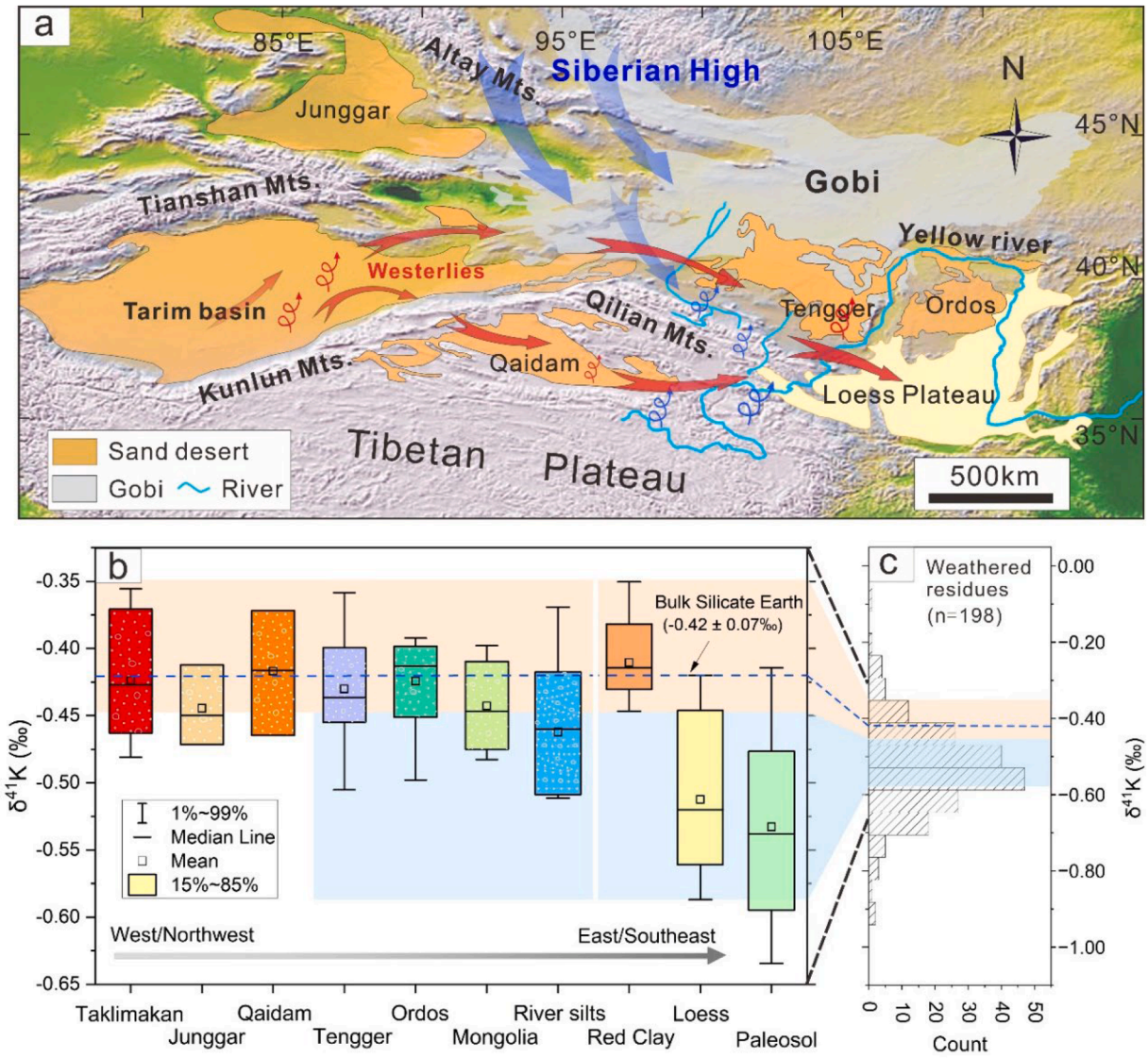

Fig. 5. Schematic illustration of East Asian atmospheric circulation and K isotope variations in potential source regions. (**a**). Schematic showing dust transport via northwesterly winds associated with the Siberian High during the Quaternary. (**b**). Box plot of δ^{41}K values of potential source materials and eolian deposits. (**c**). Histogram of compiled δ^{41}K data of the weathered products from upper continental crust. The δ^{41}K value of the bulk silicate earth (BSE) is from Hu et al. (2021).

The bulk samples and clay fractions show uniform δ^{41}K values (−0.41 ± 0.05 ‰, 2SD, n = 21) throughout the Red Clay sequence (Fig. 2), indicating thorough mixing of source materials amid the Red Clay accumulation (Ding et al., 2001). The overall distribution of δ^{41}K in potential source materials, desert silts, ranges from −0.36 ‰ to −0.51 ‰ (Fig. 5 and Table S4). Notably, the δ^{41}K values, exceeding −0.41 ‰ and comparable to that of the Red Clay, are clustered in the NTP (i.e., the eastern Tarim Basin and Qaidam Basin). These suggest that the NTP may be the primary dust source for the Red Clay. This interpretation is consistent with the view that the Taklimakan Desert was an important dust source of the CLP (Meng et al., 2019; Nie et al., 2014). The Altay mountain regions may play a role as the δ^{41}K values of Red Clay are not entirely different from those of the Mongolia and Junggar Basin samples. A recent study also suggested that the NTP contributed over 90 % of materials to the CLP since ~ 2.58 Ma (Zhang et al., 2022). Overall, the K isotope results combined with the previous knowledge suggest that the NTP is an important source for the CLP (e.g., Nie et al., 2014; Pullen et al., 2011).

Previous studies have also documented the influence of river systems in the NTP on shaping the Badain Jaran desert (Wang et al., 2015), the Tengger desert (Li et al., 2014) and the CLP (Bird et al., 2015; Nie et al., 2015; Stevens et al., 2013; Zhang et al., 2021). Indeed, the loess-like, low δ^{41}K values (−0.51 ‰ to −0.42 ‰) have been detected from the riverine sediments (Ruoshui River, Shiyang River, the upper reaches of Yellow River) in regions to the northwest of the CLP, which further supports the crucial role of river systems in the formation of the CLP. Overall, our K isotope results provide complementary constraints on dust source, showing consistence with previous studies that emphasize the contribution of deserts and fluvial systems to the formation of the CLP (e.g., Chen and Li, 2011; Nie et al., 2015).

4.3. *Generation of low-δ^{41}k source for eolian deposits since ~2.58 Ma*

The source-dominated δ^{41}K requires an isotopically light dust source to explain the lower δ^{41}K values observed in the Quaternary loess-paleosol sequence. We propose that the enhanced denudation in source regions, driven by the evolution of river system (Nie et al., 2018) and global cooling, resulted in the development of low-δ^{41}K sources for the loess deposits since ~2.58 Ma. Weathered detritus and sedimentary rocks generally have lower δ^{41}K values (down to −1.0 ‰) (Chen et al.,

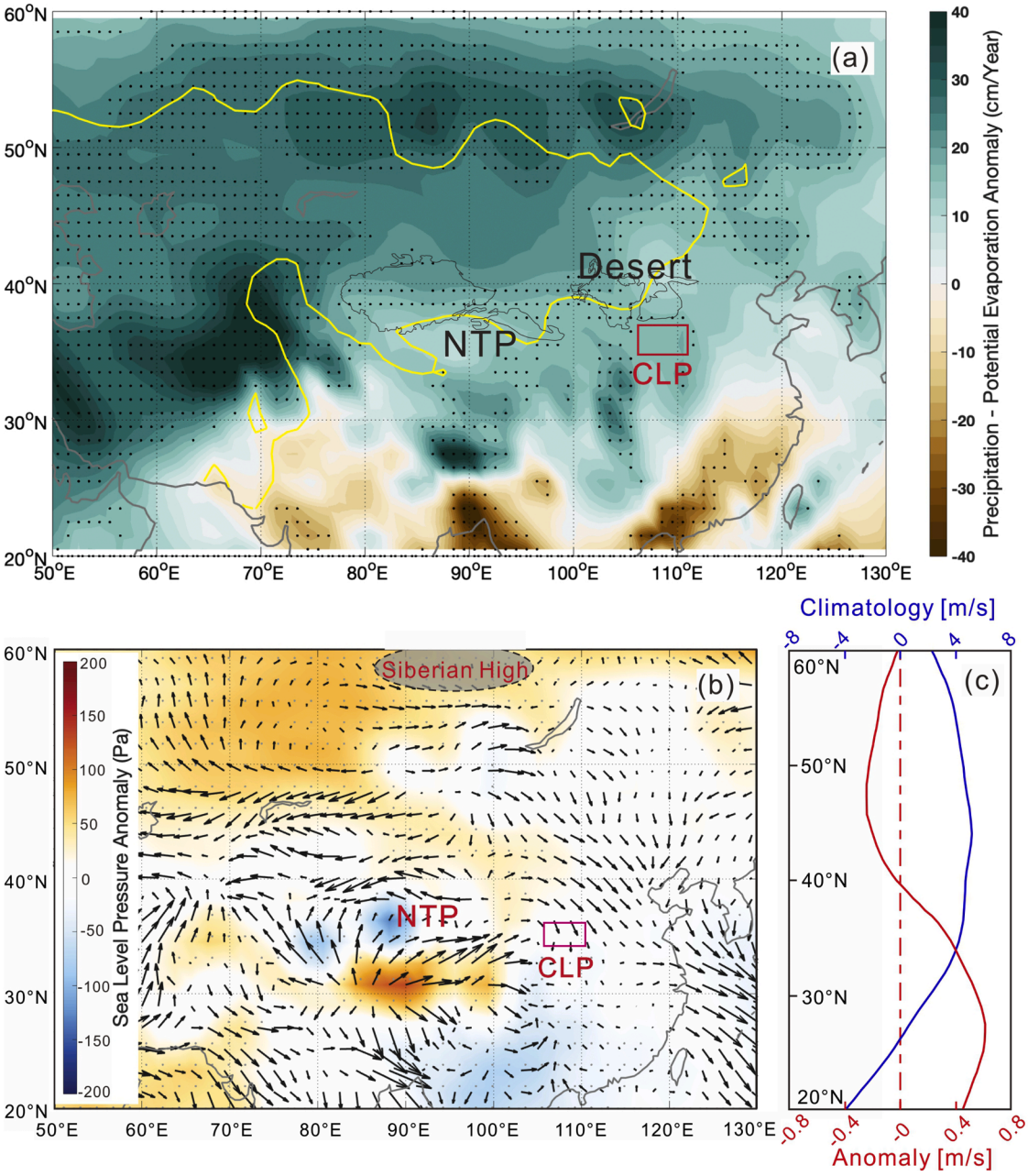

Fig. 6. Simulated changes in the moisture, surface wind and pressure in the global cooling experiment using AWI-ESM. (a). The shading color represents changes in the precipitation minus potential evaporation. The yellow contour indicates areas defined as arid zone (annual mean precipitation below 400 mm/year) before the Quaternary (pCO_2=568 ppmv). (**b**). Anomaly in pressure (shading color) and winter (Oct to April) surface winds (arrows) under low-CO_2 forcing. The stippling in panel A and B represents moisture and sea level pressure anomalies passing the 95 % confidence level (Student's *t*-test). (**c**). Panel shows the climatology zonal wind in the high-CO_2 (568 ppmv, blue line) and wind anomaly in the low-CO_2 (284 ppmv, red line) scenarios. The positive and negative values represent westerly and easterly winds, respectively. Global cooling causes an equatorward shift of westerlies, which are represented by weakened westerly wind between 40°−60°N and westerly wind anomalies at lower latitudes in the low-CO_2 scenario compared to the high-CO_2 scenario (also see Fig. S7).

2020; Huang et al., 2020; Teng et al., 2020). As noted above, low $\delta^{41}K$ values (−0.51 ‰ to −0.42 ‰) have been observed in the Tengger desert, Ordos deserts, and the riverine silt sediments from the NTP (Fig. 5). These collectively suggests the importance of river incision and riverine delivery of materials in the CLP formation (Nie et al., 2015). The lower $\delta^{41}K$ values in riverine silts were likely due to humid conditions accelerating minerals weathering along the flowing rivers. Further, we have compiled K isotope data of upper crustal materials (e.g., soils, sedimentary rocks, river sediments, and weathering profile regolith), which is particularly relevant for interpreting the $\delta^{41}K$ signature of loess, given that loess source materials are derived from vast regions of the Asian interior where such weathered crustal components are widely distributed. These upper crustal pre-weathered materials demonstrate systematically negative $\delta^{41}K$ values (−0.2 ‰ to −1.2 ‰) compared to pristine igneous rocks (Fig. 4). Thus, addition of these weathered material provides a plausible explanation for the isotopically light K observed in the loess/paleosol sequence.

It is notable that the slightly lower $\delta^{41}K$ values observed in some loess-paleosol samples, relative to desert and riverine silt, may also arise from other potential factors. 1) Post-depositional pedogenic processes may have a certain impact on decreasing K isotope values. Pedogenesis is generally characterized by neoformation of clay minerals, which tend

to incorporate the lighter K isotope (^{39}K) into their structural sites. As a result, a few samples exhibit lower δ^{41}K values. 2) The limited sample size of source materials may not be sufficient to fully capture the isotopically light K reservoirs. For instance, Li et al. (2023) reported δ^{41}K values of suspended sediments from the Lancang River on the Tibetan Plateau ranging from -0.56 ± 0.05 ‰ to -0.42 ± 0.03 ‰, consistent with the K isotope range observed in loess (-0.59 ± 0.02 ‰ to -0.43 ± 0.03 ‰). While our study analyzed the potential source materials, we recognize that some isotopically light-K-bearing reservoirs, such as sedimentary rocks, recycled paleosol and river suspended sediments, may not have been fully characterized. Future targeted sampling of these potential sources (e.g., sedimentary strata, weathering profiles at the NTP regions) will help clarify their contributions to the loess δ^{41}K signature.

The increased supply of weathered source materials were likely triggered by the late Cenozoic cooling of the Asian interior, which was linked to the major iNHG initiated at ~2.6 Ma (Bridges et al., 2023; Lu et al., 2010; Rea et al., 1998). The enhanced cooling and high relief of the NTP would have facilitated mountain processes (e.g., glacial grinding), reduced vegetation cover, and enlarged the exposure of sedimentary rocks that already experienced degrees of chemical weathering (Zhang et al., 2022). As a result, wind erosion and river transport, along with sediment recycling and reworking, were boosted (Ding et al., 1992; Licht et al., 2016; Nie et al., 2015). Indeed, wind erosion has notably impacted Yardang sedimentary strata in the Qaidam Basin, removing a volume of strata comparable to the CLP deposits (Kapp et al., 2011). Similarly, mineralogical analysis of loess particles also revealed the contribution of sedimentary clastic components (Jeong et al., 2008).On the other hand, the instability of the climate (i.e., rapid glacial-periglacial cycling) could also accelerate erosion rate (Zhang et al., 2001), thereby exposing more fresh weathering front and enhancing chemical weathering. Moreover, a long transport time (~ 240 ky) of eolian materials from source regions to the CLP can facilitate efficient chemical weathering (Li et al., 2017). Access to the increased amount of recycled and reworked sediments, characterized by δ^{41}K values lower than that of the BSE (Fig. 4), could have led to a decrease in δ^{41}K values in the loess-paleosol sequence.

The global cooling-induced changes in land surface moisture and Asian atmospheric circulation pattern also likely account for the δ^{41}K values decrease. It has been postulated that the iNHG could lead to the decline in evaporation rate, thereby increasing available moisture via higher glacial meltwater runoff (Zhang et al., 2019; Zhong et al., 2022). This hypothesis was tested herein using the AWI-ESM simulation, and the results show a net increase in terrestrial surface moisture (Fig. 6a) due to the reduction in evaporation surpassing precipitation decrease in inland Asia. A higher moisture availability was also reflected by the vegetation turnover in the Qaidam Basin, where the abundance of higher water-demanding Artemisia exceeded that of Chenopodiaceae pollen since the late Pliocene (Koutsodendris et al., 2019). Moreover, the high dust accumulation rate on the CLP was attributed to the warm-wet East Asian monsoon (Nie et al., 2018, 2015). The enhanced moisture availability could have expedited the kinetics of mineral weathering and formation of weathered fine-grained materials (Zhang et al., 2019), which were eventually blown to the CLP and North Pacific Ocean via the near-surface winds and westerlies (Lu et al., 2010; Zhang et al., 2021). Therefore, the higher moisture-driven chemical weathering in source regions, rather than utter physical erosion, provide plausible explanation concerning the observed lower δ^{41}K values in the Quaternary successions.

The drop in δ^{41}K values since the Quaternary may also reflect changes in the westerlies and Siberian High intensity over the East Asia. In the Pliocene, the westerlies likely moved poleward (Abell et al., 2021), with a weaker Siberian High causing detrital materials to come mainly from arid western regions (e.g., Taklamakan Desert, NTP) via the westerlies (Abell et al., 2021; Lu et al., 2020). In the early Quaternary, the westerlies shifted southward, while the Siberian High intensified (Lu et al., 2020; Müller et al., 2001) driven by meridional temperature gradients and iNHG (Kleiven et al., 2002; McClymont et al., 2023). This atmospheric circulation pattern was further validated through our modelling approach. Specifically, a southward shift of westerlies was observed in the Northern Hemisphere, accompanied by an intensified Siberian High due to the global cooling since the Quaternary (Fig. 6b, c and Fig. S7). This could have enhanced the transport of ^{41}K-depleted materials from proximal deserts (e.g., Alxa arid lands) and river sediments to the CLP via northwesterly winds associated with the Siberian High (Amit et al., 2014), which is consistent with observed increases in the average grain size and sedimentation rates of eolian deposits since the beginning of the Quaternary (Lu et al., 2010).

Overall, our study provided new constraints on the source materials for the CLP, revealing the crucial roles of river systems and Quaternary cooling effects on its formation, and shedding new insight into complex interplay between climatic cooling, source region dynamics, and atmospheric circulation in shaping the loess deposition processes.

5. Conclusion

On the basis of a comprehensive K isotopic analysis of the Red Clay and loess-paleosol sequences over the past ~6 million years, combined with a K isotope survey of potential source materials and Earth system modeling, we conclude:

(1) K isotope compositions of eolian deposits on the CLP exhibit dramatic decrease since the beginning of the Quaternary. The change in K isotope values cannot be attributed to post-depositional weathering. Instead, the observed K isotopic shift is governed by changes in dust source materials across the CLP over the last ~ 6 Myr.
(2) Based on the K isotope survey of potential source materials, including desert and riverine silts, our results support that the NTP serves as the dominant dust source for the CLP, with rivers also playing a crucial role in supplying weathered material to the CLP.
(3) The K isotopic shift since the Quaternary is best explained by an increased contribution of weathered detritus or recycled sediments from the NTP regions, which can be attributed to the enhanced global cooling that intensified the denudation process and altered the atmospheric circulation pattern in Asian interior across the Pliocene-Pleistocene boundary.
(4) Earth system model simulations further suggest that increased moisture availability and shifts in atmospheric circulation during the Quaternary cooling could have facilitated the generation and transport of weathered materials to the CLP, providing explanation for the observed decrease in δ^{41}K values since ~2.58 Ma.

CRediT authorship contribution statement

Jun Mu: Visualization, Writing – original draft, Investigation, Methodology, Data curation. **Jiawei Da:** Investigation, Writing – review & editing. **Hu Yang:** Writing – review & editing, Methodology. **Junfeng Ji:** Investigation, Resources, Writing – review & editing. **Lianwen Liu:** Validation, Conceptualization, Investigation. **Weiqiang Li:** Writing – review & editing, Conceptualization, Investigation, Supervision.

Declaration of competing interest

The authors declare that they have no known competing financial interests or personal relationships that could have appeared to influence the work reported in this paper.

Acknowledgments

The authors were supported by the following fundings: National

Natural Science Foundation of China 42425301 (WL); National Natural Science Foundation of China grant 42030503 (JJ); GeoX' Interdisciplinary Project of Frontiers Science Center for Critical Earth Material Cycling, Grant No. 20250103. Program B for Outstanding PhD Candidates of Nanjing University (JM). This paper benefited from constructive comments from two anonymous reviewers and editor Yemane Asmerom.

Supplementary materials

Supplementary material associated with this article can be found, in the online version, at doi:10.1016/j.epsl.2025.119543.

Data availability

All data needed to evaluate the conclusions are available in the supplementary materials.

References

Abell, J.T., Winckler, G., Anderson, R.F., Herbert, T.D., 2021. Poleward and weakened westerlies during pliocene warmth. Nature 589, 70–75.
Amit, R., Enzel, Y., Mushkin, A., Gillespie, A., Batbaatar, J., Crouvi, O., Vandenberghe, J., An, Z., 2014. Linking coarse silt production in Asian sand deserts and quaternary accretion of the Chinese Loess Plateau. Geology 42, 23–26.
An, S., Chen, J., Boschi, S., Li, W., 2023. Significantly enhanced robustness of K isotope analysis by collision cell MC-ICP-MS and its application to the returned lunar samples by China's Chang'e-5 Project. Anal. Chem. 95, 2140–2145.
An, S., Luo, X., Li, W., 2022. Precise measurement of 41K/39K ratios by high-resolution multicollector inductively coupled plasma mass spectrometry under a dry and hot plasma setting. Rapid Commun. Mass Spectrom. 36, e9289.
Bird, A., Millar, I., Rodenburg, T., Stevens, T., Rittner, M., Vermeesch, P., Lu, H., 2020. A constant Chinese Loess Plateau dust source since the late Miocene. Quat. Sci. Rev. 227, 106042.
Bird, A., Stevens, T., Rittner, M., Vermeesch, P., Carter, A., Andò, S., Garzanti, E., Lu, H., Nie, J., Zeng, L., Zhang, H., Xu, Z., 2015. Quaternary dust source variation across the Chinese Loess Plateau. Palaeogeogr. Palaeoclimatol. Palaeoecol. 435, 254–264.
Bridges, J.D., Tarduno, J.A., Cottrell, R.D., Herbert, T.D., 2023. Rapid strengthening of westerlies accompanied intensification of Northern Hemisphere glaciation. Nat. Commun. 14, 3905.
Chauvel, C., Garçon, M., Bureau, S., Besnault, A., Jahn, B.-m., Ding, Z., 2014. Constraints from loess on the Hf–Nd isotopic composition of the upper continental crust. Earth Planet. Sci. Lett. 388, 48–58.
Chen, H., Liu, X.-M., Wang, K., 2020. Potassium isotope fractionation during chemical weathering of basalts. Earth Planet. Sci. Lett. 539, 1–9.
Chen, J., Li, G., 2011. Geochemical studies on the source region of Asian dust. Sci. China Earth Sci. 54, 1279.
Chen, J., Liu, L., Ji, J., Yang, J., Chen, Y., 2001. Variation of the chemical compositions of eolian dust on the Chinese Loess Plateau and chemical weathering in Asian interior since the last 2.5 ma. Sci. China Ser. D 31, 136–145.
Chen, Z., Li, G., 2013. Evolving sources of eolian detritus on the Chinese Loess Plateau since early Miocene: tectonic and climatic controls. Earth Planet. Sci. Lett. 371-372, 220–225.
Da, J., Breecker, D.O., Li, T., Li, G., Lu, H., Ji, J., 2023. A humid East Asia during the early pliocene indicated by calcite nodules from the Chinese loess plateau. Paleoceanography and Paleoclimatology 38 e2023PA004615.
Ding, Z., Rutter, N., Jingtai, H., Tungsheng, L., 1992. A coupled environmental system formed at about 2.5 ma in East Asia. Palaeogeogr. Palaeoclimatol. Palaeoecol. 94, 223–242.
Ding, Z.L., Sun, J.M., Yang, S.L., Liu, T.S., 2001. Geochemistry of the pliocene red clay formation in the Chinese Loess Plateau and implications for its origin, source provenance and paleoclimate change. Geochim. Cosmochim. Acta 65, 901–913.
Ding, Z.L., Xiong, S.F., Sun, J.M., Yang, S.L., Gu, Z.Y., Liu, T.S., 1999. Pedostratigraphy and paleomagnetism of a ~7.0 ma eolian loess–red clay sequence at Lingtai, Loess Plateau, north-central China and the implications for paleomonsoon evolution. Palaeogeogr. Palaeoclimatol. Palaeoecol. 152, 49–66.
Guinoiseau, D., Gélabert, A., Moureau, J., Louvat, P., Benedetti, M.F., 2016. Zn isotope fractionation during sorption onto Kaolinite. Environ. Sci. Technol. 50 (4), 1844–1852.
Gylesjö, S., Arnold, E., 2006. Clay mineralogy of a red clay–loess sequence from Lingtai, the Chinese Loess Plateau. Glob Planet Change 51, 181–194.
He, T., Liu, L., Chen, Y., Sheng, X., Ji, J., 2017. A seven-million-year hornblende mineral record from the central Chinese Loess Plateau. Sci. Rep. 7, 2382.
Hu, Y., Chen, X.-Y., Xu, Y.-K., Teng, F.-Z., 2018. High-precision analysis of potassium isotopes by HR-MC-ICPMS. Chem. Geol. 493, 100–108.
Hu, Y., Teng, F.Z., Helz, R.T., Chauvel, C., 2021. Potassium isotope fractionation during magmatic differentiation and the composition of the mantle. J. Geophys. Res.: Solid Earth 126, 1–13.
Huang, T.-Y., Teng, F.-Z., Rudnick, R.L., Chen, X.-Y., Hu, Y., Liu, Y.-S., Wu, F.-Y., 2020. Heterogeneous potassium isotopic composition of the upper continental crust. Geochim. Cosmochim. Acta 278, 122–136.
Jeong, G.Y., Hillier, S., Kemp, R.A., 2008. Quantitative bulk and single-particle mineralogy of a thick Chinese loess–paleosol section: implications for loess provenance and weathering. Quat. Sci. Rev. 27, 1271–1287.
Kapp, P., Pelletier, Rohrmann, A., Heermance, R., Russell, J., Ding, L., 2011. Wind erosion in the Qaidam Basin, central Asia: implications for tectonics, paleoclimate, and the source of the Loess Plateau. GSA Today 21, 4–10.
Kleiven, F.H., Jansen, E., Fronval, T., Smith, T.M., 2002. Intensification of Northern Hemisphere glaciations in the circum Atlantic region (3.5–2.4 Ma) – ice-rafted detritus evidence. Palaeogeogr. Palaeoclimatol. Palaeoecol. 184, 213–223.
Koutsodendris, A., Allstädt, F.J., Kern, O.A., Kousis, I., Schwarz, F., Vannacci, M., Woutersen, A., Appel, E., Berke, M.A., Fang, X., Friedrich, O., Hoorn, C., Salzmann, U., Pross, J., 2019. Late Pliocene vegetation turnover on the NE Tibetan Plateau (Central Asia) triggered by early Northern Hemisphere glaciation. Glob. Planet. Change 180, 117–125.
Li, L., Chen, J., Chen, Y., Hedding, D.W., Li, T., Li, L., Liu, X., Zeng, F., Wu, W., Zhao, L., Li, G., 2018. Uranium isotopic constraints on the provenance of dust on the Chinese Loess Plateau. Geology 46, 747–750.
Li, W., Liu, X.-M., Hu, Y., Teng, F.-Z., Hu, Y.-F., Chadwick, O.A., 2021. Potassium isotopic fractionation in a humid and an arid soil–plant system in Hawai'i. Geoderma 400, 115219.
Li, L., Liu, X., Li, T., Li, L., Zhao, L., Ji, J., Chen, J., Li, G., 2017. Uranium comminution age tested by the eolian deposits on the Chinese Loess Plateau. Earth Planet. Sci. Lett. 467, 64–71.
Li, X., Han, G., Zhang, Q., Liu, J., Qu, R., 2023. Contrasting riverine K and Li isotope signatures during silicate weathering in the southeastern Tibetan Plateau. Earth Planet. Sci. Lett. 622, 118402.
Li, W., Li, S., Beard, B.L., 2019. Geological cycling of potassium and the K isotopic response: insights from loess and shales. Acta Geochimica 38, 508–516.
Li, X., Li, Y., Li, Y., Liu, M., Huang, R., Han, Z., 2025. Particle size control on loess geochemistry: characteristics, mechanisms, and implications for provenance tracing. Geochem. Geophys. Geosyst. 26 e2024GC012046.
Li, W., Liu, X.-M., Wang, K., Takahashi, Y., Hu, Y., Chadwick, O.A., 2022. Soil potassium isotope composition during four million years of ecosystem development in Hawai'i. Geochimica et Cosmochimica Acta 332, 55–77.
Li, Z., Sun, D., Chen, F., Wang, F., Zhang, Y., Guo, F., Wang, X., Li, B., 2014. Chronology and paleoenvironmental records of a drill core in the central Tengger Desert of China. Quat. Sci. Rev. 85, 85–98.
Licht, A., Pullen, A., Kapp, P., Abell, J., Giesler, N., 2016. Eolian cannibalism: reworked loess and fluvial sediment as the main sources of the Chinese Loess Plateau. GSA Bulletin 128, 944–956.
Lu, H., Wang, X., Li, L., 2010. Aeolian sediment evidence that global cooling has driven late cenozoic stepwise aridification in central Asia. In: Clift, P.D., Tada, R., Zheng, H. (Eds.), Monsoon Evolution and Tectonic–Climate Linkage in Asia. Geological Society of London, pp. 29–44.
Lu, H., Wang, X., Wang, X., Chang, X., Zhang, H., Xu, Z., Zhang, W., Wei, H., Zhang, X., Yi, S., Zhang, W., Feng, H., Wang, Y., Wang, Y., Han, Z., 2019. Formation and evolution of Gobi Desert in central and eastern Asia. Earth Sci. Rev. 194, 251–263.
Lu, Y., Dewald, N., Koutsodendris, A., Kaboth-Bahr, S., Rösler, W., Fang, X., Pross, J., Appel, E., Friedrich, O., 2020. Sedimentological evidence for pronounced glacial-interglacial climate fluctuations in NE Tibet in the latest pliocene to early pleistocene. Paleoceanography and Paleoclimatol. 35 e2020PA003864.
McClymont, E.L., Ho, S.L., Ford, H.L., Bailey, I., Berke, M.A., Bolton, C.T., De Schepper, S., Grant, G.R., Groeneveld, J., Inglis, G.N., Karas, C., Patterson, M.O., Swann, G.E.A., Thirumalai, K., White, S.M., Alonso-Garcia, M., Anand, P., Hoogakker, B.A.A., Littler, K., Petrick, B.F., Risebrobakken, B., Abell, J.T., Crocker, A.J., de Graaf, F., Feakins, S.J., Hargreaves, J.C., Jones, C.L., Markowska, M., Ratnayake, A.S., Stepanek, C., Tangunan, D., 2023. Climate evolution through the onset and intensification of Northern Hemisphere glaciation. Rev. Geophys. 61 e2022RG000793.
Meng, X., Liu, L., Zhao, W., He, T., Chen, J., Ji, J., 2019. Distant Taklimakan Desert as an important source of Aeolian deposits on the Chinese loess plateau as evidenced by carbonate minerals. Geophys. Res. Lett. 46, 4854–4862.
Morgan, L.E., Santiago Ramos, D.P., Davidheiser-Kroll, B., Faithfull, J., Lloyd, N.S., Ellam, R.M., Higgins, J.A., 2018. High-precision 41K/39K measurements by MC-ICP-MS indicate terrestrial variability of δ41K. J. Anal. At. Spectrom. 33, 175–186.
Mu, J., Chen, T., Yu, Q., An, S., Chen, J., Shi, X., Li, W., 2024. Potassium isotopic signatures of modern offshore detrital sediments from different climatic regimes and the implications. SCIENCE CHINA Earth Sciences 67, 1–9.
Müller, J., Oberhänsli, H., Melles, M., Schwab, M., Rachold, V., Hubberten, H.W., 2001. Late Pliocene sedimentation in Lake Baikal: implications for climatic and tectonic change in SE Siberia. Palaeogeogr. Palaeoclimatol. Palaeoecol. 174, 305–326.
Nie, J., Peng, W., Möller, A., Song, Y., Stockli, D.F., Stevens, T., Horton, B.K., Liu, S., Bird, A., Oalmann, J., Gong, H., Fang, X., 2014. Provenance of the upper miocene–Pliocene red Clay deposits of the Chinese loess plateau. Earth Planet. Sci. Lett. 407, 35–47.
Nie, J., Pullen, A., Garzione, C.N., Peng, W., Wang, Z., 2018. Pre-quaternary decoupling between Asian aridification and high dust accumulation rates. Sci. Adv. 4, eaao6977.
Nie, J., Stevens, T., Rittner, M., Stockli, D., Garzanti, E., Limonta, M., Bird, A., Andò, S., Vermeesch, P., Saylor, J., Lu, H., Breecker, D., Hu, X., Liu, S., Resentini, A., Vezzoli, G., Peng, W., Carter, A., Ji, S., Pan, B., 2015. Loess Plateau storage of Northeastern Tibetan Plateau-derived Yellow River sediment. Nat. Commun. 6, 8511.

Pullen, A., Kapp, P., McCallister, A.T., Chang, H., Gehrels, G.E., Garzione, C.N., Heermance, R.V., Ding, L., 2011. Qaidam Basin and northern Tibetan Plateau as dust sources for the Chinese Loess Plateau and paleoclimatic implications. Geology 39, 1031–1034.
Rae, J.W.B., Zhang, Y.G., Liu, X., Foster, G.L., Stoll, H.M., Whiteford, R.D.M., 2021. Atmospheric CO2 over the past 66 million years from marine archives. Annu. Rev. Earth Planet. Sci. 49, 609–641.
Rao, W., Yang, J., Chen, J., Li, G., 2006. Sr-Nd isotope geochemistry of eolian dust of the arid-semiarid areas in China: implications for loess provenance and monsoon evolution. Chin. Sci. Bull. 51, 1401–1412.
Rea, D.K., Snoeckx, H., Joseph, L.H., 1998. Late Cenozoic eolian deposition in the North Pacific: asian drying, Tibetan uplift, and cooling of the northern hemisphere. Paleoceanography 12, 215–224.
Sidorenko, D., Goessling, H.F., Koldunov, N.V., Scholz, P., Danilov, S., Barbi, D., Cabos, W., Gurses, O., Harig, S., Hinrichs, C., Juricke, S., Lohmann, G., Losch, M., Mu, L., Rackow, T., Rakowsky, N., Sein, D., Semmler, T., Shi, X., Stepanek, C., Streffing, J., Wang, Q., Wekerle, C., Yang, H., Jung, T., 2019. Evaluation of FESOM2.0 coupled to ECHAM6.3: preindustrial and HighResMIP simulations. J. Adv. Model. Earth Syst. 11, 3794–3815.
Stevens, T., Carter, A., Watson, T.P., Vermeesch, P., Andò, S., Bird, A.F., Lu, H., Garzanti, E., Cottam, M.A., Sevastjanova, I., 2013. Genetic linkage between the Yellow River, the Mu Us desert and the Chinese Loess Plateau. Quat. Sci. Rev. 78, 355–368.
Sun, J., 2005. Nd and Sr isotopic variations in Chinese eolian deposits during the past 8 ma: implications for provenance change. Earth Planet. Sci. Lett. 240, 454–466.
Sun, J., Zhu, X., 2010. Temporal variations in Pb isotopes and trace element concentrations within Chinese eolian deposits during the past 8Ma: implications for provenance change. Earth Planet. Sci. Lett. 290, 438–447.
Sun, Y., An, Z., Clemens, S.C., Bloemendal, J., Vandenberghe, J., 2010. Seven million years of wind and precipitation variability on the Chinese Loess Plateau. Earth Planet. Sci. Lett. 297, 525–535.
Teng, F.Z., Hu, Y., Ma, J.L., Wei, G.J., Rudnick, R.L., 2020. Potassium isotope fractionation during continental weathering and implications for global K isotopic balance. Geochim. Cosmochim. Acta 278, 261–271.
Wang, F., Sun, D., Chen, F., Bloemendal, J., Guo, F., Li, Z., Zhang, Y., Li, B., Wang, X., 2015. Formation and evolution of the Badain Jaran Desert, North China, as revealed by a drill core from the desert centre and by geological survey. Palaeogeogr. Palaeoclimatol. Palaeoecol. 426, 139–158.
Wang, Y.-X., Yang, J.-D., Chen, J., Zhang, K.-J., Rao, W.-B., 2007. The Sr and Nd isotopic variations of the Chinese Loess Plateau during the past 7 ma: implications for the East Asian winter monsoon and source areas of loess. Palaeogeogr. Palaeoclimatol. Palaeoecol. 249, 351–361.
Xiao, G., Zong, K., Li, G., Hu, Z., Dupont-Nivet, G., Peng, S., Zhang, K., 2012. Spatial and glacial-interglacial variations in provenance of the Chinese Loess Plateau. Geophys. Res. Lett. 39, L20715.
Xiong, S., Ding, Z., Zhu, Y., Zhou, R., Lu, H., 2010. A ~6Ma chemical weathering history, the grain size dependence of chemical weathering intensity, and its implications for provenance change of the Chinese loess–red clay deposit. Quat. Sci. Rev. 29, 1911–1922.
Yan, Y., Ma, L., Sun, Y., 2017. Tectonic and climatic controls on provenance changes of fine-grained dust on the Chinese Loess Plateau since the late Oligocene. Geochim. Cosmochim. Acta 200, 110–122.
Yang, S., Ding, F., Ding, Z., 2006. Pleistocene chemical weathering history of Asian arid and semi-arid regions recorded in loess deposits of China and Tajikistan. Geochim. Cosmochim. Acta 70, 1695–1709.
Yang, Y., Ye, C., Galy, A., Fang, X., Xue, Y., Liu, Y., Yang, R., Zhang, R., Han, W., Zhang, W., Ruan, X., 2021. Monsoon-enhanced silicate weathering as a new atmospheric CO2 consumption mechanism contributing to fast late miocene global cooling. Paleoceanography Paleoclimatol. 36 e2020PA004008.
Zhang, H., Lu, H., He, J., Xie, W., Wang, H., Zhang, H., Breecker, D., Bird, A., Stevens, T., Nie, J., Li, G., 2022. Large-number detrital zircon U-Pb ages reveal global cooling caused the formation of the Chinese Loess Plateau during late Miocene. Sci. Adv. 8, eabq2007.
Zhang, H., Lu, H., Xu, X., Liu, X., Yang, T., Stevens, T., Bird, A., Xu, Z., Zhang, T., Lei, F., Feng, H., 2016. Quantitative estimation of the contribution of dust sources to Chinese loess using detrital zircon U-Pb age patterns. J. Geophys. Res.: Earth Surface 121, 2085–2099.
Zhang, H., Nie, J., Liu, X., Pullen, A., Li, G., Peng, W., Zhang, H., 2021. Spatially variable provenance of the Chinese Loess Plateau. Geology 49, 1155–1159.
Zhang, P., Molnar, P., Downs, W.R., 2001. Increased sedimentation rates and grain sizes 2–4 myr ago due to the influence of climate change on erosion rates. Nature 410, 891–897.
Zhang, Q., Liu, Q., Roberts, A.P., Larrasoaña, J.C., Shi, X., Jin, C., 2019. Mechanism for enhanced eolian dust flux recorded in North Pacific Ocean sediments since 4.0 ma: aridity or humidity at dust source areas in the Asian interior? Geology 48, 77–81.
Zheng, H., An, Z., Shaw, J., 1992. New contributions to Chinese Plio-pleistocene magnetostratigraphy. Phys. Earth Planet. Inter. 70, 146–153.
Zhong, Y., Shi, X., Yang, H., Wilson, D.J., Hein, J.R., Kaboth-Bahr, S., Lu, Z., Clift, P.D., Yan, Q., Lohmann, G., Liu, J., González, F.J., Jiang, X., Jiang, Z., Liu, Q., 2022. Humidification of Central Asia and equatorward shifts of westerly winds since the late Pliocene. Commun. Earth Environ. 3, 274.
Zhou, G., Li, L., Xiao, G., Yan, L., Pearson, D.G., Hao, Q., Wu, Y., 2022. New constraints on the source of loess from U/Th-Pb geochronology of detrital multi-minerals. Geology 50, 1156–1160.